HHS Public Access

Author manuscript

Exp Neurol. Author manuscript; available in PMC 2017 January 01.

Published in final edited form as:

Exp Neurol. 2016 January ; 275(0 1): 182–198. doi:10.1016/j.expneurol.2015.09.012.

Novel p75 neurotrophin receptor ligand stabilizes neuronal calcium, preserves mitochondrial movement and protects against HIV associated neuropathogenesis

Rick B. Meeker[1], **Winona Poulton**[1,2], **Gillian Clary**[1,4], **Michael Schriver**[1], and **Frank M. Longo**[3,5]

[1]Department of Neurology, University of North Carolina, Chapel Hill, NC 27599

[3]Department of Neurology and Neurological Sciences, Stanford University School of Medicine, Stanford, CA 94305

Abstract

Human immunodeficiency virus (HIV) rapidly penetrates into the brain and establishes a persistent infection of macrophages/microglia. Activation of these cells by HIV results in the secretion of soluble factors that destabilize neuronal calcium homeostasis, encourage oxidative stress and result in neural damage. This damage is thought to underlie the cognitive-motor dysfunction that develops in many HIV-infected patients. Studies have suggested that neurotrophins may protect neurons from the toxic effects of HIV-associated proteins. To better understand the pathogenic mechanisms and the neuroprotective potential of neurotrophin ligands, we evaluated neuronal damage, calcium homeostasis and mitochondrial functions after exposure of cultured rat neurons directly to HIV gp120 or to conditioned medium from human monocyte-derived macrophages treated with gp120. We then assessed the ability of a new non-peptide p75 neurotrophin receptor ligand, LM11A-31, to stabilize calcium homeostasis and prevent the development of pathology. Each toxic challenge resulted in a delayed accumulation of intracellular calcium coupled to a decrease in the rate of calcium clearance from the cell. The delayed calcium accumulation correlated with the development of focal dendritic swellings (beading), cytoskeletal damage and impaired movement of mitochondria. Addition of LM11A-31 to the cultures at nanomolar concentrations eliminated cell death, significantly reduced the pathology, suppressed the delayed accumulation of calcium and restored mitochondrial movements. The potent neuroprotection and the stabilization of calcium homeostasis indicate that LM11A-31 may have excellent potential for the treatment of HIV-associated neurodegeneration.

Corresponding Author: Rick Meeker, Department of Neurology, CB #7025, 6109F Neuroscience Research Building, 115 Mason Farm Road, University of North Carolina, Chapel Hill, NC 27599, Phone: 919-966-5512, meekerr@neurology.unc.edu.
[2]Current Address: Winona Poulton, Durham County Department of Public Health, Durham NC 27701
[4]Now at U.S. Food and Drug Administration, Rockville, MD 20852
[5]Dr. Longo is founder of PharmatrophiX Inc., a company focused on the development of neurotrophin ligands including LM11A-31

Keywords

dementia; encephalitis; inflammation; viral infection; LM11A-31; nerve growth factor

Introduction

Human immunodeficiency virus (HIV) rapidly enters the central nervous system (CNS) where it productively infects macrophages and microglia. The presence of virus is often associated with the gradual development of a range of cognitive-motor deficits. Although combination antiretroviral therapy (CART) has decreased the severity of neurological symptoms, CNS disease continues to progress in HIV-infected patients (Gongvatana et al., 2013; Heaton et al., 2011) and evolve into different types of pathology(Brew, 2004; Gongvatana et al., 2013; Heaton et al., 2011; Langford et al., 2003; Masliah et al., 1997; Sacktor et al., 2002). Interventions are needed to suppress neuropathogenesis which, if unchecked, is expected to support an increasing neurological disease burden.

Soluble factors released in response to inflammatory activation of macrophages and microglia by the virus and viral proteins are thought to contribute substantially to the development of HIV-associated neurological deficits(Giulian et al., 1990; Kaul et al., 2001; Lipton, 1992; Pulliam et al., 1991; Xiong et al., 2000; Zheng et al., 1999). In HIV-infected patients the abundance of activated macrophages/microglia in the CNS is one of the best correlates of the severity of CNS disease(Fischer-Smith et al., 2004; Glass et al., 1995). Although the identity of the macrophage-derived toxins and the specific mechanisms of neuropathogenesis are still being defined, facilitation of NMDA glutamate receptor activity, accumulation of excess intracellular calcium and oxidative stress have been implicated(Kaul et al., 2001; Turchan et al., 2003a). Abnormal increases in intracellular calcium in neurons, in particular, may be a common underlying feature of the neurotoxic processes(Pivovarova and Andrews, 2010). Partial neuroprotection has been seen for a wide range of antagonists that block increases in intracellular calcium(Bragg et al., 2002; Dreyer et al., 1990; Holden et al., 1999) and agents that decrease oxidative stress(Turchan et al., 2003b). Various strategies are being explored to suppress inflammation and protect neurons but no approach has thus far been shown to have strong neuroprotective efficacy in clinical trials.

A promising new therapeutic strategy for neuroprotection is suggested by a loss of neurotrophic support in the context of HIV infection. An analysis of proteins in cerebrospinal fluid (CSF) from HIV infected patients showed that several neurotrophins are increased in HIV-infected, cognitively normal patients but then decrease with increasing cognitive deficits suggesting that a loss of neurotrophin protection may contribute to pathogenesis(Meeker et al., 2005). In studies that model HIV neuropathogenesis, brain-derived neurotrophic factor (BDNF) and nerve growth factor (NGF) protected neurons against Tat- (Ramirez et al., 2001) and gp120-mediated apoptosis(Bachis et al., 2006; Bachis and Mocchetti, 2005; Mocchetti and Bachis, 2004; Peruzzi et al., 2002). A large number of studies across many fields support the widespread protective and repair functions of the neurotrophins and has fostered considerable work on their therapeutic use. However,

these efforts have been limited by difficulties with stability, access to the CNS and side effects(Allen et al., 2013).

The recent development of a new class of neurotrophin ligands has made it possible to examine the efficacy of novel non-peptide compounds that modify neurotrophin receptor function. The prototype neurotrophin ligand for our studies, LM11A-31, is a small molecule selected to mimic the loop 1 region of NGF, a domain known to bind the p75 neurotrophin receptor ($p75^{NTR}$)(Longo et al., 2007). This compound has been shown to have neurotrophic activity and promote Akt-1 signaling(Massa et al., 2006). The following studies examined the potential of LM11A-31 to protect cultured neurons from the damaging effects of HIV gp120 and macrophage-generated toxins.

Materials and Methods

Neural cultures

Neural cultures were prepared from the cortex/hippocampus of E17 rat fetuses. Pregnant female Long-Evans rats were lethally anesthetized with isoflurane and the uterus removed and placed in ice cold HEPES-buffered Hank's balanced salt solution (HBSS). The brain was harvested from each fetus, rinsed three times in fresh sterile HBSS and the forebrain containing the cortex, hippocampus and basal ganglia transferred to a 15 ml tube containing calcium-magnesium free HBSS (CMF-HBSS), 1.25 U/ml dispase II + 2 U/ml DNase I. After incubation for 25–30 min at 37° C the cells were gently dissociated by several rounds of trituration and seeded into poly-D-lysine-coated culture dishes at a density of 50,000 – 100,000 cells/cm^2 for toxicity analysis or 20,000 cells/cm^2 on poly-D-lysine-treated coverslips for imaging. The resulting cultures were typically >90% neurons at 6 days in culture (average value for representative cultures was 96 ± 2% neurons). Cultures were fed with Minimum Essential Medium (MEM) with glutamine, 10% fetal bovine serum and 20 μg/ml gentamicin, 50% exchange, three times per week. Cells were allowed to grow at least 6 days *in vitro*, at which time they show extensive synaptophysin immunoreactivity and excellent responses to gp120, macrophage-conditioned medium and glutamate receptor agonists.

Initially, a challenge with the HIV envelope protein gp120 (200 pM) was selected to assess neuroprotection due to previously demonstrated effects on neurotrophins and the large body of data available for the toxic effects of this protein. To determine the most effective stimulus and the earliest changes associated with neural damage, different strains of gp120 were compared using intracellular calcium accumulation and cell death as endpoints. This comparison helped to rule out the possibility that toxicity and protective effects may be unique to particular subtypes of gp120. The effects of the gp120 were also contrasted to the toxic effects previously seen with CSF from HIV-infected patients(Meeker et al., 2005) to determine if similar toxic effects were present. In addition, gp120 was applied to monocyte-derived macrophages with subsequent testing of the conditioned medium on neural cultures. A direct comparison of the toxicity of the conditioned medium to direct application of gp120 showed that the conditioned medium produced similar effects but was much more potent. Thus, the neuroprotective effects of LM11A-31 in the sensitive calcium assays were assessed using the more potent conditioned medium.

Sources and types of gp120

Since both CXCR4- and CCR5-preferring subtypes of gp120 have been shown to be toxic to neurons but may have slightly different actions(Kaul et al., 2007), we compared the pathogenic effects of each subtype to determine if there was a common effect leading to neural dysfunction. Four subtypes of gp120 were obtained from the AIDS Reference Reagent Program. Two subtypes, $gp120_{IIIB}$ and $gp120_{MN}$ represented CXCR4-preferring subtypes and two subtypes, $gp120_{BaL}$ and $gp120_{SF162}$ represented CCR5-preferring subtypes. A separate supply of full length, glycosylated $gp120_{LAV}$ (sequence similar to $gp120_{IIIB}$) was also obtained from Protein Sciences (Meriden, CT). The $gp120_{IIIB}$ and $gp120_{LAV}$ both yielded similar effects. A challenge concentration of 200 pM was chosen based on previous work(Digicaylioglu et al., 2004; Dreyer et al., 1990; Garden et al., 2002; Kaul and Lipton, 1999; Meucci and Miller, 1996). To avoid multiple freeze-thaw cycles, a 100X stock was prepared in an artificial CSF (aCSF, concentrations in mM: NaCl 137, KCl 5.0, $CaCl_2$ 2.3, $MgCl_2$ 1.3, glucose 20, HEPES 10, adjusted to pH 7.4 with NaOH), aliquoted and stored frozen until use. In some experiments, lipopolysacchraride (LPS 0.1 μg/ml) and rat interferon-γ (INF, 20 U/ml) were applied to the cultures to provide a strong positive control for inflammatory damage.

Conditioned medium from human monocyte-derived macrophages (hMDM)

Human peripheral blood mononuclear cells (PBMCs) from healthy donors were purchased from the New York Blood Center (Long Island City, NY). Research was approved by the center prior to acquisition and the blood was shipped with no identifiers of any kind. Approximately 10^8 PBMCs were obtained, washed and cultured in DMEM + 10% FBS in 6-well plates on low adhesion plastic. Monocytes were allowed to adhere for a period of 5–7 days after which they were transferred to DMEM containing 15 ng/ml recombinant human granulocyte-macrophage colony stimulating factor (GM-CSF, R&D Systems, Minneapolis, MN) and differentiated for an additional 5 days. After differentiation the macrophages were returned to DMEM + 10% fetal bovine serum. These mature macrophages were then washed and treated with 200 pM gp120 in 2 mls DMEM + 1% FBS per well (without GM-CSF) for a period of 3 days. The resulting medium was collected, aliquoted and stored at −80°. Cultures treated identically but with no gp120 stimulation were used as controls.

For MDM-neuron co-cultures, rat MDM were isolated from 14–16 mls of blood and cultured in a similar fashion. Cells were harvested from the low adhesion plates in calcium-magnesium free Hank's Balanced Salt Solution (CMF-HBSS) at 4° C (~20–30 min), centrifuged and the pellet re-suspended in aCSF at a density of 5000 cells/ml at room temperature. The cells were then seeded onto the neuronal cultures at a density of approximately 1000 cells/cm^2 (4% of the neuron density) to observe direct interactions of macrophages with neurons.

Measurement of cell death

To assess cell death in response to a challenge, the live culture was stained by adding 1 μM ethidium homodimer to the medium for a period of 20 min followed by washing and fixation in 70% ethanol. Nuclei of dead cells show an intense red fluorescence. In some experiments nuclei were stained with 0.5–1 μM bisbenzimide (Hoechst 33258) or Sytox green for double

labeling studies. Counting of dead cells was accomplished by systematically sampling the left, right, top, bottom and middle of each well at an image magnification of 195X. The five readings were then averaged to provide a single value for each well. Metamorph Image Analysis software (Molecular Devices, Union City, CA) was used to identify stained nuclei using brightness and object size discriminators. The total number of objects that met the criteria for a stained nucleus was automatically counted. This procedure provided a relatively unbiased estimate of the stained nuclei for approximately 18% of the total surface of each well of a 96 well plate, representing approximately 2800 total neurons.

Immunocytochemistry

Neurons were identified by microtubule-associated protein-2 (MAP-2) immunostaining. Cells were fixed in ice cold 97% methanol, 3% acetic for 10 min at room temperature and washed in 0.01 M phosphate-buffered saline (PBS, 3×5 min). After incubation in blocking buffer containing 3% normal goat serum in 0.01 M PBS for 60 min polyclonal rabbit anti-MAP-2 (Chemicon/Millipore, Bilerica, MA) was applied at a dilution of 1:500 in blocking buffer and incubated overnight at 4°C. The cells were washed three times in PBS and incubated in biotinylated goat anti-rabbit at 1:500 for 1 h at room temp or goat anti-rabbit Alexa488 (1:500) or mouse anti-rabbit Alexa568 (1:500). The cells were washed three times in PBS. Cells with the biotinylated secondary antibody were incubated for 1 h at room temp in avidin-Alexa488 (1:500, Molecular Probes/Invitrogen, Carlsbad, CA) and then washed 3×5 min. Nuclei were counterstained with bisbenzimide (0.5 μM, Sigma Corp, St Louis, MO) for 20 min in PBS, washed 2×5 min and the coverslips were mounted onto slides with Fluoromount (Southern Biotech, Birmingham AL). A similar protocol was followed for staining of phospho-Akt (pAkt) and phospho-cyclic AMP response element binding protein (pCREB).

Staining was examined with an Olympus IMT-2 or IX71 inverted microscope and quantified with digital imaging and Metamorph (Molecular Devices, Downingtown, PA) imaging software. Fluorescence brightness intensity was measured at magnifications of 334X and 674X and the density of neurons and processes was quantified using the threshold and intensity functions. Images were collected from pre-determined regions of the coverslip and analyzed by an individual unaware of the treatment conditions. The total area occupied by MAP-2 immunoreactive cell bodies and processes was measured and expressed as a percentage of the entire field and the average pAkt and pCREB stain intensity for the MAP-2 positive neurons was measured. Data was collected from individual neurons at high magnification and the population distributions and average intensity of the neurons compared across conditions. Intensity values were corrected for background measured in regions that did not contain cells. Astrocytes were also weakly positive for pAkt and pCREB but were not measured (MAP-2 negative).

LM11A-31: a non-peptide neurotrophin ligand

The compound LM11A-31 was initially identified by Drs. Longo and Massa using a virtual screen of a small molecule library to identify compounds mimicking the spatial and physical chemical features of the loop 1 region of NGF, a domain known to bind to $p75^{NTR}$ (Massa et al., 2002). Subsequent screening of compounds showed LM11A-31 to have neurotrophic

activity, high affinity for $p75^{NTR}$, and the ability to activate downstream signaling via PI3 kinase and Akt(Massa et al., 2002; Massa et al., 2006) with no direct actions on the nerve growth factor receptor, TrkA or the brain-derived neurotrophic factor receptor, TrkB. LM11A-31, has potent neuroprotective properties under conditions of serum starvation with EC_{50} values of 200–300 pM and a maximally effective concentration of 5–100 nM in various assays(Massa et al., 2006; Yang et al., 2008).

Calcium imaging

Neuronal cultures were washed in HEPES-buffered artificial CSF (aCSF, concentrations in mM: NaCl 137, KCl 5.0, $CaCl_2$ 2.3, $MgCl_2$ 1.3, glucose 20, HEPES 10, adjusted to pH 7.4 with NaOH) and pre-loaded with the calcium indicator, Fluo-3 AM or Fluo-4 AM using the Molecular Probes Fluo-4 NW Calcium Assay Kit (Molecular Probes/Invitrogen, Eugene, OR) at a 1:4 dilution. After 30 minutes, cultures were washed in aCSF and 18 mm coverslips mounted in a specialized stage for imaging (Warner Instruments, Hamden, CT). Images were captured on an Olympus IX71 inverted microscope at a temperature of 25° which provided stable background activity for at least 2 hrs. LM11A-31 was added to the coverslips in the chamber 10 min prior to the challenge. The cells were challenged with 200 pM gp120 final concentration or conditioned medium from hMDM treated for 3 days with 200 pM gp120. The toxic challenge was added in a volume of 80 μl to 320 μl in the chamber to provide a 1:5 dilution of the stock. Time lapse digital images were captured automatically by the Metamorph System (Molecular Devices, Union City, CA). Three pre-stimulation measurements were taken to establish basal levels of fluorescence at the beginning of each experiment. Acute changes in calcium were measured at 0.1 min intervals for 6 min. Delayed changes in calcium were measured at 1 min intervals for at least an additional 60 min. The increase in fluorescence intensity (free calcium) within each cell was then measured relative to the baseline measurements to correct for cell to cell differences in dye loading and intrinsic fluorescence. Control cultures were stimulated with vehicle or control medium (medium from same hMDM cultures prior to the challenge with gp120) in the same fashion to establish normal baseline calcium activity as well as any intrinsic toxic activity from the hMDM cultures.

Imaging of mitochondria with JC-1 and TMRM

To measure changes in the mitochondrial membrane potential, neural cultures were loaded with JC-1 dye (Molecular Probes/Invitrogen) at a concentration of 3 μM in complete medium for 30 min at 36°. Cells were washed with aCSF, placed in an imaging chamber and challenged with a 1:5 dilution of toxic human CSF previously shown to cause substantial calcium dysregulation. The red and green fluorescence was measured in individual mitochondria with narrow bandpass filters at 6–12 minute intervals over a period of 96 min. The average green:red ratio was calculated and plotted over time. Polarized healthy mitochondria have a low green:red ratio and the ratio increases with depolarization. Fluo-3 fluorescence, reflecting intracellular calcium, was measured in parallel cultures under the same conditions and plotted over the same time period for a temporal comparison to changes in mitochondrial membrane potential.

Experiments were also done using cells loaded with 10 nM tetramethlyrhodamine methyl ester (TMRM) to label mitochondria. TMRM was added to the cells for 10 min at the end of the 30 min loading period for the calcium indicator Fluo-4. Cells were washed in aCSF, and the mitochondria imaged. The cells were then challenged with conditioned medium from gp120-stimulated human MDM (1:5). Fluorescence of the calcium indicator was measured over time. Regions of dendrites where swelling occurred were then compared to the location of mitochondria to determine if there was a relationship between the presence of mitochondria and damage.

Mitochondria movements were tracked by labeling with 10 nM TMRM for 10 min followed by addition of the MCM challenge with or without drug. Time lapse images were collected over a period of 30 min. Imaging was initiated in some studies immediately after stimulation with macrophage conditioned medium while in other studies the cells were pre-incubated for period of 30 min to allow the development of pathology. No changes in TMRM fluorescence were seen as a result of immediate MCM treatment or after incubation for 30 min verifying that there were no acute effects on the mitochondrial membrane potential.

Statistics

Results are presented as the mean ± sem unless otherwise indicated. Parametric statistics, ANOVA for multiple comparisons and t-test for single comparisons, were calculated using Graphpad Prism software. In the case of multiple comparisons the ANOVA was followed by specific individual paired comparisons to correct for the multiple comparisons. In some cases t-tests were run on two comparisons without correction when there was a single main effect and a secondary comparison to validate stimulus effectiveness. A cutoff of 0.05 was accepted as significant. Estimates of calcium recovery rates were obtained from linear regression analysis of the log transformation of calcium (fluorescence) levels relative to the peak response. The probability of equal slopes was calculated from the individual regression lines.

Results

Comparison of the neurotoxic effects of gp120 and macrophage conditioned medium

To provide a stringent and valid test of the actions of our neurotrophin ligand we utilized several toxic challenges and pathological endpoints that mimic effects seen in HIV-infected humans. Since gp120 is a well characterized stimulus that produces neurotoxicity we initially evaluated interactions of LM11A-31 with gp120-induced neurotoxicity. Because subtypes of gp120 may have differential effects in neural cultures we compared the effects of both CXCR4-preferring ($gp120_{IIIB}$, $gp120_{MN}$) and CCR5-preferring ($gp120_{BaL}$ and $gp120_{SF162}$) subtypes to identify the optimal challenge and to determine if there were notable differences between HIV subtypes in our paradigm. Neural cultures were treated with 200 pM gp120 and cell death measured at 24 h. Figure 1A illustrates the cell death seen with each subtype of gp120. All subtypes were toxic relative to vehicle controls and resulted in an average cell death ranging from 67.2 to 85.3 cells/mm^2 versus 18.4 cells/mm^2 for vehicle controls (all p values < 0.006 for gp120 vs. control). The relative extent of cell death for the gp120 treated cultures ranged from 5.1 ± 1.0% to 6.5 ± 0.5% of total neurons versus

1.4 ± 0.2% for control cultures. While the increases in cell death represented 3.6 – 4.6 fold increases over control values it is important to note that most neurons in the culture did not die under these conditions.

To evaluate the neuroprotective efficacy of LM11A-31, neural cultures were incubated as above with 200 pM $gp120_{IIIB}$ in the presence or absence of 10 nM LM11A-31. To provide a strong positive control, a separate set of cultures was treated with a potent inflammatory stimulus, lipopolysaccharide (LPS 0.1 μg/ml) + rat interferon-γ (INF, 20 U/ml). Under these conditions gp120 induced a 152% increase in cell death and the LPS + γ-interferon a 494% increase in cell death relative to vehicle treated controls (Figure 1B). Co-treatment with 10 nM LM11A-31 completely reversed the cell death in both cases, resulting in less cell death than vehicle-treated controls.

Previous studies of CSF from HIV-infected patients had indicated that delayed calcium destabilization was an early and sensitive index of toxicity(Meeker et al., 2005). To determine if each gp120 subtype also caused similar changes in calcium homeostasis, we evaluated the direct effect of each of four subtypes of gp120 on neuronal intracellular calcium regulation and the response to a glutamate challenge. As illustrated in Figure 2A, a negligible or small acute rise in intracellular calcium was seen followed by a gradual accumulation starting at approximately 10–20 min. By 60 min, an average rise of 117.1 – 155.0% (±7.6 – 13.1%) was seen relative to 4.8 ± 3.8% in vehicle controls. All subtypes of gp120 produced similar effects on intracellular calcium. In seven independent experiments, the percentage of cells showing a dysregulation of intracellular calcium during exposure to gp120 was 67.1 ± 5.3%. Thus, under these conditions most neurons are dysfunctional although few die as a result of the challenge (4–5%).

To evaluate the ability of neurons to clear a calcium load after exposure to gp120, mixed neural cultures were incubated with each type of gp120 for three days followed by an acute 2 s challenge with 200 μM glutamate with rapid washout. The acute response to a pulse of glutamate, shown in Figure 2B, was increased in all cells treated with gp120 (271 – 445% increase above basal) relative to cells treated with vehicle (aCSF, 136.0% increase above basal). Although peak levels varied slightly, between gp120 subtypes, ($gp120_{BaL}$ 445.5 ± 35.5%; $gp120_{MN}$ 404.0 ± 36.2%; $gp120_{IIIB}$ 280.0 ± 21.6%; and $gp120_{SF162}$ 271.3 ± 22.9%) the pattern was the same for each. The increase in the acute calcium response was paralleled by a decrease in the rate of recovery as seen previously for CSF from HIV-infected patients and feline cultures infected with FIV(Bragg et al., 2002; Meeker et al., 2005). The ratio of fluorescence values at each time point (F) to the peak calcium (F_{peak}) was calculated and log transformed to determine the rate of recovery (slope). After a slight delay of 12–18 s, all gp120 treated cells showed slower calcium recovery rates relative to untreated cells (Figure 2C). The mean recovery rate for control cells was 4.43% s^{-1} versus 0.89% s^{-1} (IIIB), 0.83% s^{-1} (SF162), 0.95% s^{-1} (BaL), and 1.10% s^{-1} (MN), representing 4- to 5-fold decreases in calcium clearance.

Since the increased acute calcium response to glutamate after exposure to gp120 could contribute to the changes seen in the clearance rate we compared calcium clearance rates in cells with similar calcium loads. When the acute responses to a 2 s pulse of glutamate in

$gp120_{IIIB}$-treated cells was matched to control cells (Figure 2D), a delay in calcium recovery was still evident in the gp120-treated cells. The corresponding plot of the transformed data in Fig 2D (inset) illustrates that the rate of recovery was 5-fold less than control cells even with the same acute calcium burden.

Since the toxic effects of gp120 may be largely due to interactions with macrophages and microglia, we also treated human monocyte-derived macrophages (hMDM) with 200 pM gp120 for a period of three days and examined the effects of the secreted products on neuronal calcium homeostasis. Macrophage conditioned medium (MCM) was applied to cultures at dilutions of 1:20, 1:10, 1:5 and 1:2.5. A linear dose-response relationship was seen between the concentration of conditioned medium and neuronal calcium accumulation assessed at 40 min, the approximate midpoint of the delayed rise. Fluorescence increases ranged from 47.6 ± 12.0 fluorescence units at a 1:10 dilution to 196.4 ± 12.0 fluorescence units at a 1:2.5 dilution (not shown, all p's<0.05). The MCM, at a dilution of 1:5, produced a delayed increase in intracellular calcium (Figure 3A) that was typically 2–3 fold greater that that seen with gp120 alone. However, in contrast to gp120 alone, a large acute calcium response was seen. The acute calcium increase recovered only partially before the development of the delayed increase. Similar patterns were seen with medium from hMDM treated with $gp120_{IIIB}$ or $gp120_{BaL}$ again indicating little strain difference in the generation of a toxic response from macrophages. Although not necessary or sufficient for the development of the late rise, the acute rise appeared to facilitate the delayed response. Since glutamate in the conditioned medium was a candidate for the cause of the acute calcium rise, we measured the concentration in the MCM. Glutamate was present in the conditioned medium at an average concentration of 4.1 ± 0.5 μM (n=5 separate experiments). In our assay, with a medium dilution of 1:5 the glutamate delivered to the cultures was, on average, 0.82 μM. Stimulation of the cultures directly with 0.82 μM glutamate, shown in Figure 3B, produced a rapid calcium rise followed by complete recovery by 2 min and no significant long-term destabilization. Thus, glutamate in the medium contributes to the initial calcium burden but could not account for the destabilization of calcium homeostasis. It is important to note that the glutamate concentration in the medium was not static. Fresh medium contained 12.9 ± 0.11 μM glutamate which was rapidly reduced to a steady state value of 4 μM with a $t_{1/2}$ of 2.95 h.

To further verify the toxic activity of the macrophages under conditions that mimic *in vivo* interactions, rat MDM (rMDM) treated with either $gp120_{IIIB}$ or $gp120_{BaL}$ were seeded into normal neural cultures at a low density to evaluate local interactions between the rMDM and neurons. After 24 h, macrophages were observed next to neurons. Figure 4 A–C illustrates several images of MAP-2 stained neurons (green) from the same culture with various levels of damage. Healthy neurons were seen in regions with no rMDM (Figure 4A) while neurons in the vicinity of rMDM (red) showed damage ranging from early signs of beading (Figure 4B) to severe dendritic swelling, perikaryon shrinkage and pruning of processes (Figure 4C). Unchallenged macrophages did not produce damage (not shown) and in some cases appeared to facilitate neuronal growth suggesting a beneficial influence in the absence of an inflammatory challenge.

LM11A-31 protects neurons from the effects of macrophage-derived toxins

Since conditioned medium from macrophages treated with gp120 produced greater neuronal damage and a much more robust destabilization of calcium than gp120 alone, we evaluated the ability of LM11A-31 to protect neurons challenged with human MCM at a dilution of 1:5 for 24 h. Total MAP-2 immunostaining was used to provide an index of changes in neuronal architecture. As illustrated in Figure 5, treatment of the cultures with MCM resulted in a 32.2% loss of MAP-2 immunoreactivity relative to untreated cultures or vehicle treated cultures ($p=0.00013$). The loss of MAP-2 stain in the presence of MCM was largely due to a decrease in the area occupied by MAP-2+ processes with an additional but smaller contribution from decreased staining of the neuronal cell bodies. Addition of 10 nM LM11A-31 to the culture medium 10 min prior to the MCM challenge totally prevented the loss of MAP-2 staining ($p=0.0073$ vs. MDM; 14% greater MAP-2 than control). An example of neurons damaged by MCM and the reversal of the damage by 2 nM and 10 nM LM11A-31 is shown in Figure 6A–C. The cultures treated with MCM showed dendritic beading and some pruning of processes (Figure 6A). Treatment with LM11A-31 at 2 nM partially restored the neuronal morphology (Figure 6B) and at 10 nM resulted in near-normal, healthy-looking neurons with abundant processes (Figure 6C).

To determine if this neuroprotection might be due to the stabilization of intracellular calcium we measured acute and delayed calcium changes in response to MCM. As summarized in Figures 7 and 8, the addition of 10 nM LM11A-31 to the cultures 10 minutes prior to addition of the MCM (1:5) had no effect on the peak acute calcium rise but facilitated recovery and strongly suppressed the delayed calcium rise. An example of the acute and delayed changes in intracellular calcium following application of MCM (1:5) in the absence or presence of 10 nM LM11A-31 (MCM+LM11A-31) is illustrated in Figure 7A. In the absence of LM11A-31, the MCM induced a large rapid rise in calcium at 0.1 min, very little recovery (3 min) and a large delayed destabilization of calcium (60 min, movie S1). The delayed calcium destabilization was associated with the development of dendritic beading and swelling of the perikaryon. In contrast, delayed calcium accumulation and the accompanying damage were suppressed in the cultures pre-treated with LM11A-31 (Fig 7B, MCM+LM11A-31) with no effect on the acute calcium response (movie S2). Figure 7C illustrates, at higher magnification, the local calcium accumulation associated with neuritic beading. The average changes in intracellular calcium are illustrated in Figure 8A–C. Maximum recovery of calcium in the presence of LM11A-31 relative to aCSF was 91.6% at 10 min versus 37.0% in the absence of the neurotrophin ligand. The delayed destabilization of calcium was reduced from a peak of 264 ± 16 fluorescence units in the cultures treated with MCM to 67 ± 7. The background calcium destabilization in aCSF treated cells was 5.0 ± 4.6. Because the MCM might contain small amounts of residual gp120, we stimulated the cultures with $gp120_{IIIB}$ at the maximum possible concentration in the medium under the same conditions. A very small acute response was seen followed by a small gradual rise in intracellular calcium to 64.9 units above baseline. In addition, removal of the gp120 by ultrafiltration at 100 kDa had no effect on the MCM-induced neuronal calcium response (not shown). Calcium recovery following the acute peak in neurons treated with the MCM plus LM11A-31 was 3.3 times faster than the recovery rate for neurons treated with MDM-conditioned medium alone (Figure 8B). To evaluate whether astrocytes or neurons might

also generate soluble toxins in response to gp120, conditioned medium was prepared from mixed neural cultures in the same fashion. As illustrated in 8C, this medium stimulated an acute rise in calcium but failed to trigger a delayed destabilization and damage. Quantification of the extent of beading during the calcium runs is illustrated in Figure 8D. In each case, pre-stimulation images were used to correct for any pre-existing varicosities or artifacts. The images of the varicosities were digitally filtered by size to specifically identify beading of the processes and the number of varicosities was normalized to the number of neurons in the field to correct for any differences due to cell density. The extent of beading at the end of the calcium run was negligible for neurons treated with aCSF (0.016 ± 0.036 varicosities/neuron) and slightly increased by exposure to MCM collected prior to treatment with gp120 (MCM control, 0.271 ± 0.026). Conditioned medium from macrophages treated with gp120 increased beading to an average of 2.668 ± 0.644 varicosities/neuron ($p= 0.0021$ vs. MCM control). Co-treatment of neurons with MCM and 10 nM LM11A-31 resulted in a reduction of the beading to 0.158 ± 0.081 varicosities/neuron, a 95% reversal relative to MCM ($p=0.023$). In addition, if cultures were returned to complete medium with or without LM11A-31 just after the development of beading an almost full recovery was seen within 24–48 h indicating that these early pathological changes were reversible.

LM11A-31 signaling and neuroprotection

To begin to understand the signaling events that might be responsible for the observed neuroprotection, we examined neuronal changes in MAP-2, phospho Akt (pAkt) and phosphoCREB (pCREB). Neurons were identified by the MAP-2 stain and the effects of MCM were examined after 4 h and 20 h exposure. Examples of the pAkt and MAP-2 stain at 20 h post challenge and the merged images are illustrated in Figure 9A–I. After 4 h in conditioned medium, we measured a 25.1% reduction in the total MAP-2 stain (Figure 9J). Co-treatment with LM11A-31 had no significant effect on the total MAP-2 stain at this time. However, after 20 h, the loss of MAP-2 (28.7%, Fig 9D) was significantly reversed by the LM11A-31 (Fig 9G) to a level greater than the normal control neurons ($p<0.001$, Fig 9J). This time-dependent reversal indicated that the restoration of MAP-2 by LM11A-31 was gradual.

We next examined neuronal expression of pAkt, a primary intermediate in protective neurotrophin signaling. Neurons were co-stained with pAkt (Fig 9A,D,G, 20 h) and MAP-2 (Fig 9B,E,H, 20 h). At 4 h, pAkt was increased 135% in neurons in response to the MCM challenge suggesting that the neurons mount an early protective response (Figure 9K). This increase in pAkt was unaffected by co-treatment with LM11A-31 (140% above controls). At 20 h into the challenge (Fig 9A–I), the neurons treated with MCM expressed pAkt at a level 15.6% below control values ($p=0.0019$) whereas the neurons co-treated with LM11A-31 maintained an average expression of pAkt at a level 69% above the untreated control neurons ($p<0.0001$) indicating an increased ability to sustain Akt signaling in the presence of LM11A-31. Since the stain for pAkt was not as distinctive as the other stains, these results were confirmed by Western blot of the entire culture (not shown) which paralleled the changes in Fig 9K. Phosphorylation of CREB is a major downstream effect that could mediate also protection. Total pCREB did not change significantly in MCM-treated neurons at 4 h in the presence or absence of LM11A-31. After 20h, total pCREB expression (Fig

10A,D,G) decreased in the cultures treated with MCM (Fig 9D,J). Addition of LM11A-31 with the MCM (Fig 9G–I) significantly increased pCREB expression above the MCM treated cultures ($p<0.0001$, Fig 9J). Thus, the protective response of LM11A-31 was also associated with sustained pCREB expression.

Calcium, pathology and mitochondrial dysfunction

The earliest sign of pathology was the development of focal varicosities in the dendrites (beading). To better understand the temporal relationship between calcium changes and the development of pathology, we compared the development of focal swelling to local changes in dendrite intracellular calcium. An analysis of 140 swellings from 5 experiments revealed that 97.8% of these regions showed a calcium rise prior to the development of swelling. On average, the calcium rise preceded the development of swelling by 20.0 ± 1.0 min. The calcium response associated with swelling varied from cell to cell but generally fell into two categories illustrated in Figures 11A and 11B. Some processes showed small acute increases in calcium (fluorescence) followed by a rapid rise (Cell 40-1). The superimposed box (dashed lines) illustrates where the swelling of the process occurs. Other processes (Cell 59-2) showed a steady, continuous rise in calcium.

Since the appearance of focal swelling has been linked in some studies to mitochondrial dysfunction(Greenwood et al., 2007), we also examined the temporal relationship between calcium accumulation, mitochondrial depolarization and beading. The time course of calcium destabilization and the loss of the mitochondrial membrane potential were tracked over time in cultures treated with a 1:5 dilution of HIV+ human CSF previously selected for toxic activity. Fluo-3 was used to track calcium changes and an increase in the JC-1 green:red ratio was used to assess mitochondrial depolarization. To facilitate comparison, each curve was normalized to the maximum fluorescence (% of maximum signal) or the maximum change in the green:red ratio seen after depolarization of the mitochondria with 1 μM FCCP. The average normalized responses, summarized in Figure 11C, showed a transient hyperpolarization of the mitochondria (decrease in the green:red ratio) followed by a depolarization. However, by the time mitochondrial depolarization began to change significantly from baseline, at 48 min, the destabilization of calcium had reached 92% of its maximum value. These data indicate that calcium dysregulation precedes the loss of the mitochondrial membrane potential and is likely to be a more proximal cause of neuronal dysfunction. Focal swelling, however, occurred in a time frame consistent with the onset of mitochondrial depolarization. We therefore asked if mitochondria were localized to the regions of swelling to determine if there was a direct relationship between the two. TMRM stained mitochondria (Fig 12B) were mapped along the length of selected dendrites with prominent beading (Fig 12A) and superimposed on the location of varicosities (Fig 12C). Location maps were constructed (Fig 12D) representing 549 swellings. Although examples of overlap were seen as illustrated in Fig 12D, swellings occurred in the apparent absence of mitochondria (arrow) and mitochondria were often not associated with swelling. On average, 47.6% of the swellings were associated with mitochondria indicating a lack of concordance between the mitochondria and swelling. However, mitochondria that were localized to swellings often had a condensed morphology and were occasionally seen in unusual circular configurations within the swelling (Fig 12C, arrow) suggesting a disruption

of normal structure and transport. Because TMRM is dependent on an intact mitochondrial membrane potential we reasoned that the visibility of the mitochondria might be lost if they depolarize within the swellings. When we fixed the cells and stained for the mitochondrial marker Tomm20 (Fig 12E, green) the proportion of swellings (MAP-2, red) with mitochondria based on the dendritic mapping analysis (Fig 12F) increased to 94.3%. Clusters of stained mitochondria were uniquely seen in the swellings (arrows) suggesting an accumulation of depolarized mitochondria.

MCM-induced alterations in the cytoskeleton

Staining of MCM-treated neurons for F-actin with Alexa488-phalloidin revealed a dense accumulation of F-actin masses within the swellings indicating a disruption of the cytoskeleton (Fig 13A, B). Dense accumulations of actin were also seen in growth cones (Fig 13D) as compared to control cultures (Fig 13C). Similar changes have been seen in models of Alzheimer disease where the pruning of synapses and dendrites were hypothesized to be due to a loss of microtubule transport functions(Shahpasand et al., 2012; Zempel and Mandelkow, 2012). Although the relationship between the actin cytoskeleton and microtubules is not clear both have been implicated in the movement of mitochondria and neurotrophin containing vesicles(Lazarov et al., 2007; Stokin et al., 2005). To determine if transport was impaired in our model, we labeled the mitochondria with TMRM and measured both the movements and mitochondrial fluorescence intensity (membrane potential) over time. Movement maps representing the velocity of sequential movements of 50 randomly selected mitochondria from control cultures or cultures treated for 20 min with MCM are illustrated in Figs. 14A and B. A total of 1157 mitochondrial movements were measured in the control neurons and 864 movements in the neurons treated with MCM. Periods of rapid movement are illustrated by the spikes of activity for individual 6 s epochs. Rapid variation in the height of adjacent spikes illustrates the stop and go nature of the movements. Mitochondria in the control neurons had many more high velocity movements than the MCM treated cells. A comparison of the mean velocity in neurons treated with vehicle, MCM or MCM+LM11A-31, summarized from three independent experiments, is illustrated in Figure 14C. The average velocity of mitochondrial movement decreased by 52.2% in the presence of MCM relative to control cells ($p=0.0015$)(movie S3). Addition of 10 nM LM11A-31 to the medium reversed the deficit ($p=0.0044$ MDM+LM11A-31 vs. MDM) and restored the movement of the mitochondria to control values (movie S4). TMRM intensity, a measure of the mitochondrial membrane potential, showed little overall change in the MCM-treated cells (Fig. 12D). However, a small increase in TMRM intensity was seen in control cells and LM11A-31 treated cells relative to the MCM-treated cells (MCM slope = +0.01495% min^{-1} vs +0.03876% min^{-1} for control neurons, $p<0.0001$). After addition of LM11A-31 to the medium the TMRM intensities were not significantly different from controls, again indicating no effect on the mitochondrial membrane potential. Since the movement and function of mitochondria may be associated with fusion or fission events, we evaluated the size of individual mitochondria over time (Fig. 14E). All mitochondria showed a reduction in apparent size over time but no differences were seen across all conditions. As noted above, mitochondrial movements that could be localized to swellings revealed aberrant patterns of movement such as small, non-productive back and

forth movements or circular movements within the swelling reinforcing the idea that a loss of transport may underlie the development of pathology.

Discussion

Calcium deregulation is an early determinant of neural dysfunction

The results from these studies support the important role of altered intracellular calcium homeostasis in the early development of neural dysfunction in response to HIV. Addition of HIV+ CSF, gp120 or MCM to the neural cultures all disrupted long-term calcium homeostasis with MCM showing the most potent effects. Both CXCR4 and CCR5 preferring strains of gp120 produced toxic effects albeit with slightly different potencies as previously described(Kaul et al., 2007). In each case, the gp120 resulted in a destabilization of intracellular calcium that correlated with a decrease in the rate of intracellular calcium recovery. The high activity of MCM relative to other challenges reinforces the view that macrophages/microglia are a primary source of factors that produce neurotoxicity. In addition, the strong similarity between effects of MCM and CSF from HIV infected patients (Meeker et al., 2005; Meeker et al., 1999) indicates that similar conditions exist *in vivo*.

The delayed destabilization of calcium was apparent within 20 min and preceded the depolarization of mitochondria under the same conditions. The delayed calcium rise was often seen in the absence of a strong acute calcium response indicating that the neuronal dysfunction was not secondary to a strong initial accumulation of calcium. In addition, when the acute calcium rise in the MCM treated neurons was matched to control neurons the late destabilization was seen only for the MCM treated cells. This differs from excitotoxic models(Tymianski et al., 1993) where a large initial calcium rise driven by a high concentration of glutamate is thought to play major role in the late destabilization. A notable difference between the gp120 alone and MCM was the presence of an acute elevation of intracellular calcium with application of the conditioned medium, likely due to the presence of a low concentration of glutamate in the MCM. When we challenged the neurons with the same concentration of glutamate a large acute response was seen but it was not sufficient to produce delayed calcium destabilization and pathology. The decreased rate of calcium recovery seen in these experiments is consistent with previous studies showing that that the delayed destabilization of calcium correlates with the inability to remove calcium from the cytosol(Besancon et al., 2008; Bragg et al., 2002; Meeker et al., 2005). This deficit would be consistent with the gradual accumulation of intracellular calcium.

Calcium, actin and the regulation of mitochondrial movement

Calcium accumulation was closely followed by focal neuritic swelling (beading). Dendritic beading and synaptic pruning are common to a number of neurodegenerative conditions(Greenwood et al., 2007; Sanchez-Varo et al., 2012; Takeuchi et al., 2005) but little is known about the mechanisms that lead to this pathology. Mitochondrial dysfunction has been implicated in some studies(Greenwood et al., 2007). Although it was difficult to find mitochondria moving into regions of swellings in the live imaging experiments, immunostaining for the mitochondrial marker Tomm20 revealed the presence of mitochondria and in some cases an accumulation of mitochondria. These observations

suggested that, upon entering a swelling, mitochondria rapidly lose their membrane potential. The loss of mitochondrial function might then provoke focal swelling(Greenwood et al., 2007). However, the precise relationship between calcium dysregulation, the loss of transport and development of swellings is not known. While uncontrolled accumulation of calcium in our studies reflects an early deficit in neuronal function that may set the stage for subsequent degenerative changes, further work is needed to clearly identify the mechanistic link between calcium dysregulation and neuronal damage. Calcium-dependent changes in the cytoskeleton are a prominent possibility as suggested by the appearance of disorganized F-actin. There are strong similarities between the dendritic pathology seen in our studies and neuritic beading seen in early Alzheimer pathogenesis where a disruption of microtubule transport has also been implicated as an early deficit(Shah et al., 2009; Stokin et al., 2005). Calcium-mediated changes in the cytoskeleton may be common to both neurodegenerative processes. The essential role of calcium in morphological plasticity including control of spine morphology is well established(Ackermann and Matus, 2003; Bonhoeffer and Yuste, 2002; Ciani and Salinas, 2008; Fortin et al., 2010; Oertner and Matus, 2005). Changes in actin that determine spine movements and shape are regulated by calcium in a fashion that is both concentration and duration dependent. For example, normal entry of calcium through NMDA receptors and voltage-gated calcium channels, necessary for LTP, suppresses actin turnover and stabilizes spines through actin polymerization(Ackermann and Matus, 2003; Oertner and Matus, 2005) yet, under excitotoxic conditions that induce high, prolonged levels of calcium, F actin and spine structure are lost within as little as five minutes(Oertner and Matus, 2005). Similar effects are likely to influence transport functions. Future studies are needed to firmly establish the relationship between calcium regulation and structural plasticity in response to inflammatory disease.

Although an understanding of the relationship between calcium, actin, microtubules and organelle transport is still evolving, several studies provide support for the role of actin in control of mitochondrial movements. Inhibition of actin polymerization by cytochalasin D decreased the number of mitochondria moving in axons and dendrites and induced focal aggregation of actin(Ligon and Steward, 2000). The formation of actin-cofilin aggregates interfered with mitochondrial movements and was associated with synaptic loss and decreased MAP-2 expression(Cichon et al., 2012). Loss of transport has also been linked in some studies to a reduction in neurotrophic support(Lazarov et al., 2007). Chada and Hollenbeck(Chada and Hollenbeck, 2004) showed that neurotrophins may provide localization signals since mitochondria accumulated in regions next to NGF coated beads. Recent studies of van den Berg and Hoogenraad (van den Berg and Hoogenraad, 2012) indicated that short final movements involved in docking and cargo binding may follow actin filaments by a process dependent on PI3K. Thus calcium and neurotrophin signaling may function in parallel to control mitochondrial movements through interactions with actin. The actin destabilizing effects of high concentrations of calcium are qualitatively similar to the effects of $p75^{NTR}$ activation which cause neurite and growth cone retraction through a mechanism that involves the sequential activation of RhoA, ROCK and LIM-kinase(Davies, 2000; Lu et al., 2009; Yamashita et al., 1999). Thus, signaling interactions between calcium and neurotrophins are likely to play a role in the regulation of the cytoskeleton and transport (Getz, 2012; Higuchi et al., 2012; Watkins et al., 2012).

LM11A-31 neuroprotection

The ability to control neurotrophin signaling has the potential to provide neuroprotection via a wide range of processes including control of actin-dependent processes(Adalbert et al., 2007; Salehi et al., 2000). In Alzheimer disease models, deleterious effects on actin and loss of dendritic complexity may be facilitated by $p75^{NTR}$ and suppressed by TrkA (Berardi et al., 2007; Costantini et al., 2005). Pharmacological disruption of proNGF maturation to NGF shifts the signaling bias toward $p75^{NTR}$ and induces cholinergic degeneration and cognitive decline in rats(Allard et al., 2012). Importantly, early neuritic damage in 4–6 month-old AD PS1(M146L)/APP(751SL) mice that precedes synaptic and neuron loss is associated with cytoskeletal defects, actin-cofilin rods, autophagic vacuoles within axonal swellings and decreased expression of the transport motors kinesin-1 and dynein(Sanchez-Varo et al., 2012). The similarities to the neuronal pathology seen in the current experiments suggest a common neurodegenerative mechanism that could be restored by intervention with neurotrophin ligands.

The strong neuroprotective efficacy of the neurotrophin ligand, LM11A-31, seen in our studies indicates that regulation of $p75^{NTR}$ function can have potent therapeutic utility. These protective effects are consistent with the neuroprotective efficacy seen in other model systems where LM11A-31 has been shown to protect neurons *in vitro* against the toxic effects of amyloid-β_{1-42} aggregates(Yang et al., 2008) and the apoptotic effects of pro-nerve growth factor(Massa et al., 2006). Studies examining the mechanism of action of LM11A-31 have shown PI3K-dependent activation of Akt-1 and NFκB(Massa et al., 2006). Downstream inhibition of GSK-3β, calpain/CDK5 and c-Jun activation and the preservation of CREB phosphorylation may contribute to the beneficial effects of this ligand(Yang et al., 2008). In our studies, it is notable that the restoration of MAP-2 stained architecture followed the early appearance of damage, highlighting the reversibility of the deficits. The restorative effects may be due in part to the sustained activation of pAkt and pCREB in neurons treated with LM11A-31. The relatively rapid stabilization of calcium by LM11A-31 early in the pathogenic cascade may also contribute independently to the high neuroprotective potency of LM11A-31. By preventing the corresponding disruption of actin, the transport of mitochondria is preserved (and possibly other organelles and molecules). Although more work is needed to better understand the precise mechanisms of protection by LM11A-31, it is clear that novel neurotrophin ligands have unique and potent therapeutic actions that may target the earliest stages of neurodegeneration.

Supplementary Material

Refer to Web version on PubMed Central for supplementary material.

Acknowledgments

This work was supported by NIH grants MH079726 and MH085606

References

Ackermann M, Matus A. Activity-induced targeting of profilin and stabilization of dendritic spine morphology. Nature neuroscience. 2003; 6:1194–200. [PubMed: 14555951]

Adalbert R, et al. Abeta, tau and ApoE4 in Alzheimer's disease: the axonal connection. Trends in molecular medicine. 2007; 13:135–42. [PubMed: 17344096]

Allard S, et al. Impact of the NGF maturation and degradation pathway on the cortical cholinergic system phenotype. The Journal of neuroscience : the official journal of the Society for Neuroscience. 2012; 32:2002–12. [PubMed: 22323714]

Allen SJ, et al. GDNF, NGF and BDNF as therapeutic options for neurodegeneration. Pharmacology & therapeutics. 2013; 138:155–75. [PubMed: 23348013]

Bachis A, et al. Axonal transport of human immunodeficiency virus type 1 envelope protein glycoprotein 120 is found in association with neuronal apoptosis. The Journal of neuroscience : the official journal of the Society for Neuroscience. 2006; 26:6771–80. [PubMed: 16793884]

Bachis A, Mocchetti I. Brain-Derived Neurotrophic Factor Is Neuroprotective against Human Immunodeficiency Virus-1 Envelope Proteins. Ann NY Acad Sci. 2005; 1053:247–257. [PubMed: 16179530]

Berardi N, et al. Environmental enrichment delays the onset of memory deficits and reduces neuropathological hallmarks in a mouse model of Alzheimer-like neurodegeneration. Journal of Alzheimer's disease : JAD. 2007; 11:359–70. [PubMed: 17851186]

Besancon E, et al. Beyond NMDA and AMPA glutamate receptors: emerging mechanisms for ionic imbalance and cell death in stroke. Trends in pharmacological sciences. 2008; 29:268–75. [PubMed: 18384889]

Bonhoeffer T, Yuste R. Spine motility. Phenomenology, mechanisms, and function. Neuron. 2002; 35:1019–27. [PubMed: 12354393]

Bragg DC, et al. Destabilization of neuronal calcium homeostasis by factors secreted from choroid plexus macrophage cultures in response to feline immunodeficiency virus. Neurobiology of disease. 2002; 9:173–86. [PubMed: 11895370]

Brew BJ. Evidence for a change in AIDS dementia complex in the era of highly active antiretroviral therapy and the possibility of new forms of AIDS dementia complex. AIDS. 2004; 18(Suppl 1):S75–S78. [PubMed: 15075501]

Chada SR, Hollenbeck PJ. Nerve growth factor signaling regulates motility and docking of axonal mitochondria. Current biology : CB. 2004; 14:1272–6. [PubMed: 15268858]

Ciani L, Salinas PC. From neuronal activity to the actin cytoskeleton: a role for CaMKKs and betaPIX in spine morphogenesis. Neuron. 2008; 57:3–4. [PubMed: 18184558]

Cichon J, et al. Cofilin aggregation blocks intracellular trafficking and induces synaptic loss in hippocampal neurons. The Journal of biological chemistry. 2012; 287:3919–29. [PubMed: 22184127]

Costantini C, et al. Characterization of the signaling pathway downstream p75 neurotrophin receptor involved in beta-amyloid peptide-dependent cell death. Journal of molecular neuroscience : MN. 2005; 25:141–56. [PubMed: 15784962]

Davies AM. Neurotrophins: neurotrophic modulation of neurite growth. Current biology : CB. 2000; 10:R198–200. [PubMed: 10712898]

Digicaylioglu M, et al. Erythropoietin protects cerebrocortical neurons from HIV-1/gp120-induced damage. NeuroReport. 2004; 15:761–3. [PubMed: 15073510]

Dreyer E, et al. HIV-1 coat protein neurotoxicity prevented by calcium channel antagonists. Science. 1990; 248:364–367. [PubMed: 2326646]

Fischer-Smith T, et al. Macrophage/microglial accumulation and proliferating cell nuclear antigen expression in the central nervous system in human immunodeficiency virus encephalopathy. Am J Pathol. 2004; 164:2089–2099. [PubMed: 15161643]

Fortin DA, et al. Long-term potentiation-dependent spine enlargement requires synaptic Ca2+-permeable AMPA receptors recruited by CaM-kinase I. The Journal of neuroscience : the official journal of the Society for Neuroscience. 2010; 30:11565–75. [PubMed: 20810878]

Garden GA, et al. Caspase cascades in human immunodeficiency virus-associated neurodegeneration. The Journal of neuroscience : the official journal of the Society for Neuroscience. 2002; 22:4015–24. [PubMed: 12019321]

Getz GS. Calpain Inhibition as a Potential Treatment of Alzheimer's Disease. The American journal of pathology. 2012

Giulian D, et al. Secretion of neurotoxins by mononuclear phagocytes infected with HIV-1. Science. 1990; 250:1593–6. [PubMed: 2148832]

Glass JD, et al. Immunocytochemical quantitation of human immunodeficiency virus in the brain: correlations with dementia. Ann Neurol. 1995; 38:755–762. [PubMed: 7486867]

Gongvatana A, et al. Progressive cerebral injury in the setting of chronic HIV infection and antiretroviral therapy. Journal of NeuroVirology. 2013; 19:209–18. [PubMed: 23613008]

Greenwood SM, et al. Mitochondrial dysfunction and dendritic beading during neuronal toxicity. The Journal of biological chemistry. 2007; 282:26235–44. [PubMed: 17616519]

Heaton RK, et al. HIV-associated neurocognitive disorders before and during the era of combination antiretroviral therapy: differences in rates, nature, and predictors. Journal of NeuroVirology. 2011; 17:3–16. [PubMed: 21174240]

Higuchi M, et al. Mechanistic involvement of the calpain-calpastatin system in Alzheimer neuropathology. FASEB journal : official publication of the Federation of American Societies for Experimental Biology. 2012; 26:1204–17. [PubMed: 22173972]

Holden CP, et al. Role of Na+/H+ exchangers, excitatory amino acid receptors and voltage- operated Ca2+ channels in human immunodeficiency virus type 1 gp120- mediated increases in intracellular Ca2+ in human neurons and astrocytes. Neuroscience. 1999; 91:1369–1378. [PubMed: 10391443]

Kaul M, et al. Pathways to neuronal injury and apoptosis in HIV-associated dementia. Nature. 2001; 410:988–94. [PubMed: 11309629]

Kaul M, Lipton SA. Chemokines and activated macrophages in HIV gp120-induced neuronal apoptosis. Proceedings of the National Academy of Sciences of the United States of America. 1999; 96:8212–6. [PubMed: 10393974]

Kaul M, et al. HIV-1 coreceptors CCR5 and CXCR4 both mediate neuronal cell death but CCR5 paradoxically can also contribute to protection. Cell death and differentiation. 2007; 14:296–305. [PubMed: 16841089]

Langford TD, et al. Changing patterns in the neuropathogenesis of HIV during the HAART era. Brain Pathology. 2003; 13:195–210. [PubMed: 12744473]

Lazarov O, et al. Impairments in fast axonal transport and motor neuron deficits in transgenic mice expressing familial Alzheimer's disease-linked mutant presenilin 1. The Journal of neuroscience : the official journal of the Society for Neuroscience. 2007; 27:7011–20. [PubMed: 17596450]

Ligon LA, Steward O. Role of microtubules and actin filaments in the movement of mitochondria in the axons and dendrites of cultured hippocampal neurons. The Journal of comparative neurology. 2000; 427:351–61. [PubMed: 11054698]

Lipton S. Requirement of macrophages in neuronal injury induced by HIV envelope protein gp120. NeuroReport. 1992; 3:913–915. [PubMed: 1421098]

Longo FM, et al. Small molecule neurotrophin receptor ligands: novel strategies for targeting Alzheimer's disease mechanisms. Current Alzheimer research. 2007; 4:503–6. [PubMed: 18220511]

Lu Q, et al. Signaling through Rho GTPase pathway as viable drug target. Current medicinal chemistry. 2009; 16:1355–65. [PubMed: 19355891]

Masliah E, et al. Dendritic injury is a pathological substrate for human immunodeficiency virus-related cognitive disorders. HNRC Group. The HIV Neurobehavioral Research Center. Ann Neurol. 1997; 42:963–972. [PubMed: 9403489]

Massa SM, et al. Alzheimer's therapeutics: neurotrophin small molecule mimetics. Journal of molecular neuroscience : MN. 2002; 19:107–11. [PubMed: 12212765]

Massa SM, et al. Small, nonpeptide p75NTR ligands induce survival signaling and inhibit proNGF-induced death. The Journal of neuroscience : the official journal of the Society for Neuroscience. 2006; 26:5288–300. [PubMed: 16707781]

Meeker RB, et al. Cerebrospinal fluid from human immunodeficiency virus--infected individuals facilitates neurotoxicity by suppressing intracellular calcium recovery. Journal of NeuroVirology. 2005; 11:144–56. [PubMed: 16036793]

Meeker RB, et al. Neurotoxicity of CSF from HIV-infected humans. J Neurovirology. 1999; 5:507–518. [PubMed: 10568888]

Meucci O, Miller RJ. gp120-induced neurotoxicity in hippocampal pyramidal neuron cultures: protective action of TGF-beta1. J Neurosci. 1996; 16:4080–4088. [PubMed: 8753870]

Mocchetti I, Bachis A. Brain-derived neurotrophic factor activation of TrkB protects neurons from HIV-1/gp120-induced cell death. Critical reviews in neurobiology. 2004; 16:51–7. [PubMed: 15581399]

Oertner TG, Matus A. Calcium regulation of actin dynamics in dendritic spines. Cell Calcium. 2005; 37:477–82. [PubMed: 15820396]

Peruzzi F, et al. Tat-induced deregulation of neuronal differentiation and survival by nerve growth factor pathway. Journal of NeuroVirology. 2002; 8(Suppl 2):91–6. [PubMed: 12491158]

Pivovarova NB, Andrews SB. Calcium-dependent mitochondrial function and dysfunction in neurons. The FEBS journal. 2010; 277:3622–36. [PubMed: 20659161]

Pulliam L, et al. Human immunodeficiency virus-infected macrophages produce soluble factors that cause histological and neurochemical alterations in cultured human brains. J Clin Invest. 1991; 87:503–512. [PubMed: 1671392]

Ramirez SH, et al. Neurotrophins prevent HIV Tat-induced neuronal apoptosis via a nuclear factor-kappaB (NF-kappaB)-dependent mechanism. J Neurochem. 2001; 78:874–889. [PubMed: 11520908]

Sacktor N, et al. HIV-associated cognitive impairment before and after the advent of combination therapy. J Neurovirol. 2002; 8:136–142. [PubMed: 11935465]

Salehi A, et al. P75 neurotrophin receptor in the nucleus basalis of meynert in relation to age, sex, and Alzheimer's disease. Experimental Neurology. 2000; 161:245–58. [PubMed: 10683291]

Sanchez-Varo R, et al. Abnormal accumulation of autophagic vesicles correlates with axonal and synaptic pathology in young Alzheimer's mice hippocampus. Acta Neuropathologica. 2012; 123:53–70. [PubMed: 22020633]

Shah SB, et al. Examination of potential mechanisms of amyloid-induced defects in neuronal transport. Neurobiology of disease. 2009; 36:11–25. [PubMed: 19497367]

Shahpasand K, et al. Regulation of mitochondrial transport and inter-microtubule spacing by tau phosphorylation at the sites hyperphosphorylated in Alzheimer's disease. The Journal of neuroscience : the official journal of the Society for Neuroscience. 2012; 32:2430–41. [PubMed: 22396417]

Stokin GB, et al. Axonopathy and transport deficits early in the pathogenesis of Alzheimer's disease. Science. 2005; 307:1282–8. [PubMed: 15731448]

Takeuchi H, et al. Neuritic beading induced by activated microglia is an early feature of neuronal dysfunction toward neuronal death by inhibition of mitochondrial respiration and axonal transport. The Journal of biological chemistry. 2005; 280:10444–54. [PubMed: 15640150]

Turchan J, et al. Oxidative stress in HIV demented patients and protection ex vivo with novel antioxidants. Neurology. 2003a; 60:307–314. [PubMed: 12552050]

Turchan J, et al. Neuroprotective therapy for HIV dementia. Curr HIV Res. 2003b; 1:373–383. [PubMed: 15049424]

Tymianski M, et al. Source specificity of early calcium neurotoxicity in cultured embryonic spinal neurons. The Journal of neuroscience : the official journal of the Society for Neuroscience. 1993; 13:2085–104. [PubMed: 8097530]

van den Berg R, Hoogenraad CC. Molecular motors in cargo trafficking and synapse assembly. Advances in experimental medicine and biology. 2012; 970:173–96. [PubMed: 22351056]

Watkins GR, et al. Monoubiquitination Promotes Calpain Cleavage of the Protein Phosphatase 2A (PP2A) Regulatory Subunit alpha4, Altering PP2A Stability and Microtubule-associated Protein Phosphorylation. The Journal of biological chemistry. 2012; 287:24207–15. [PubMed: 22613722]

Xiong H, et al. HIV-1 infected mononuclear phagocyte secretory products affect neuronal physiology leading to cellular demise: relevance for HIV-1-associated dementia. J Neurovirol. 2000; 6(Suppl 1):S14–S23. [PubMed: 10871761]

Yamashita T, et al. Neurotrophin binding to the p75 receptor modulates Rho activity and axonal outgrowth. Neuron. 1999; 24:585–93. [PubMed: 10595511]

Yang T, et al. Small molecule, non-peptide p75 ligands inhibit Abeta-induced neurodegeneration and synaptic impairment. PloS one. 2008; 3:e3604. [PubMed: 18978948]

Zempel H, Mandelkow EM. Linking amyloid-beta and tau: amyloid-beta induced synaptic dysfunction via local wreckage of the neuronal cytoskeleton. Neuro-degenerative diseases. 2012; 10:64–72. [PubMed: 22156588]

Zheng J, et al. Lymphotropic virions affect chemokine receptor-mediated neural signaling and apoptosis: implications for human immunodeficiency virus type 1-associated dementia. Journal of Virology. 1999; 73:8256–67. [PubMed: 10482576]

Highlights

- Changes in calcium in response to a variety of different HIV-associated challenges reflect a gradual accumulation due to a dysregulation of calcium recovery.
- The gradual calcium increase precedes the development of structural pathology such as beading and is associated with a loss of actin structure and transport function.
- These pathological changes mimic early neuronal pathology for other neurodegenerative diseases potentially revealing a common underlying mechanism.
- The cellular pathology and calcium changes are reversed by the novel neurotrophin ligand, LM11A-31, providing a neurotrophin-based option for early intervention.
- These studies help to clarify the causes of neural damage induced by HIV infection and establish the p75 neurotrophin receptor as a valuable target for the treatment of HIV-associated neurodegeneration.

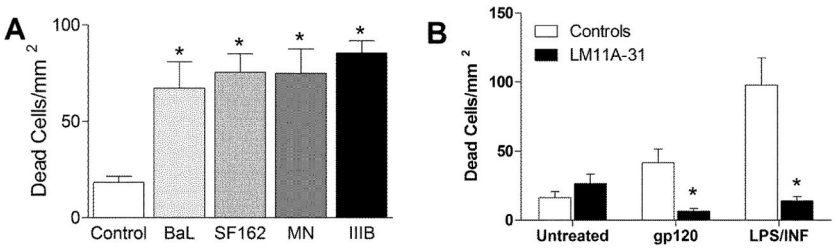

Figure 1.

Cell death and calcium changes induced by different subtypes of HIV-1 gp120 in primary rat mixed neural cultures. A. Neurons were treated with 200 pM gp120 for a period of 24 h. Cell death was assessed using ethidium homodimer to stain dead cell nuclei. The number of dead cells/mm^2 was increased for all gp120 subtypes. Cell death ranged from 1.4 ± 0.2% of total neurons in the control cultures to a maximum of 6.5 ± 0.5% for gp120$_{IIIB}$. Values represent the mean ± sem. * $p<0.05$ relative to control (One way ANOVA followed by individual paired comparisons, n=9). B. Co-incubation with 10 nM LM11A-31 prevented gp120-induced cell death in cultures treated with 200 pM gp120 or strong inflammatory stimulation with lipopolysaccharide (LPS, 0.1 μg/ml) and rat interferon-γ (INF, 20 U/ml LPS). *$p<0.01$ t-test, treatment vs. no treatment, (n=8).

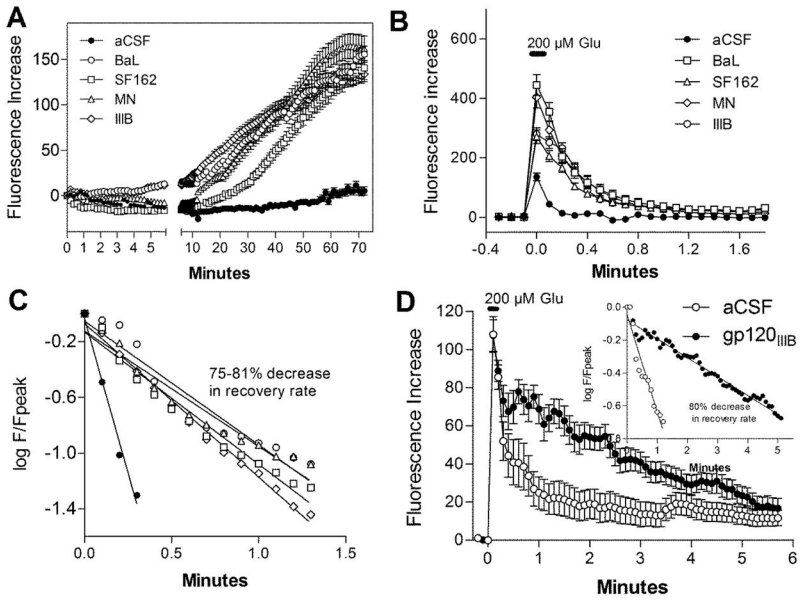

Figure 2.

A. Incubation of neural cultures with CXCR4-preferring subtypes of gp120 (IIIB, MN) or CCR5-preferring subtypes (BaL, SF162) all provoked gradual increases in intracellular calcium (Fluorescence Increase). B. Chronic treatment of neural cultures with gp120 for 3 days resulted in an increased calcium response to a 2 s pulse of glutamate. C. Fluorescence values (F) at each post-stimulation time point were normalized to the peak calcium (Fpeak) and then plotted as log F/Fpeak versus time to provide an estimate of the rate of recovery. A 75–81% reduction in the rate of recovery of intracellular calcium was seen after exposure to gp120. D. The decrease in calcium recovery persisted when neurons were matched for acute calcium load (10 control, 10 gp120). Inset: An average decrease in recovery rate of 80% was seen with calcium load matched. Data points are mean ± sem (n=20–47 neurons from at least three independent studies).

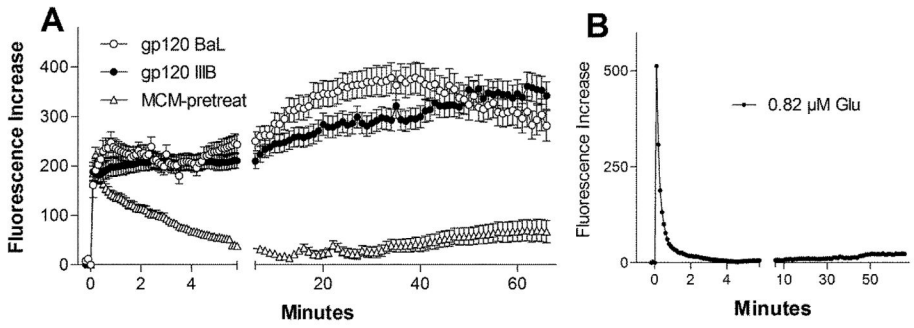

Figure 3.

Rat neural cultures challenged with medium from human monocyte-derived macrophages (hMDM) treated for three days with 200 pM $gp120_{IIIB}$ or $gp120_{BaL}$. A. The macrophage conditioned medium (MCM) was added at a dilution of 1:5 at 0 min and produced a large acute rise in intracellular calcium (Fluorescence Increase) followed by minimal recovery and a delayed destabilization of intracellular calcium. No difference was seen between medium from MCM treated with $gp120_{IIIB}$ (47 cells) or $gp120_{BaL}$ (30 cells). Medium collected from hMDM prior to treatment with gp120 (MCM-pretreat) produced a similar acute rise in intracellular calcium but only a small delayed rise (179 cells). Results represent 3–7 independent experiments. B. Single example of the response to glutamate at the same concentration present in the MCM. A similar acute response was observed which rapidly recovered to baseline with no plateau or delayed rise.

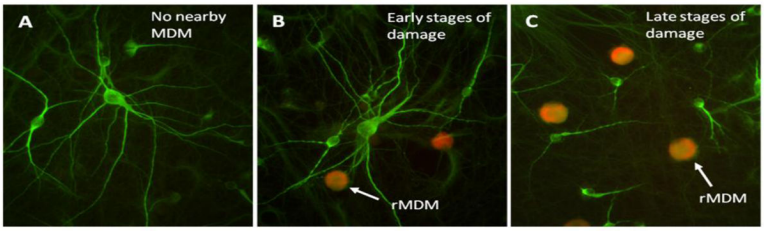

Figure 4.

Neuronal damage induced by addition of a low density of rat MDM (rMDM, 1000 cells/cm^2) which were pre-treated for 24 h with 200 pM $gp120_{IIIB}$ and then labeled with DiI acetylated LDL. Neurons stained with MAP-2 (green) could be visualized in the same regions as the rMDM (red). A. With no rMDM nearby or in the absence of rMDM (not shown), the neurons displayed normal morphology. When localized next to rMDM neurons showed different levels of damage ranging from early signs of dendritic beading (B) to prominent dendritic beading with truncation of processes (C).

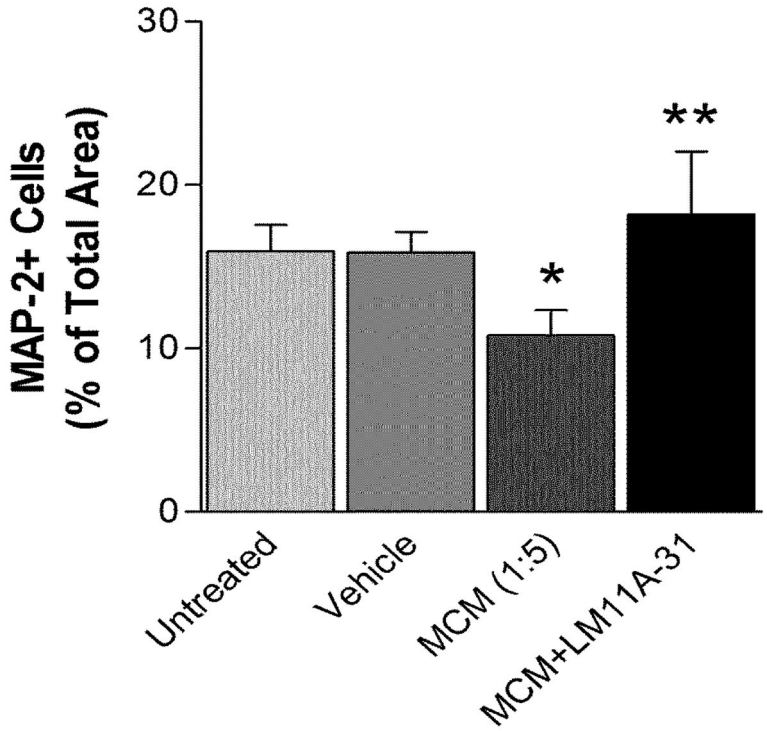

Figure 5.

The p75 neurotrophin receptor ligand, LM11A-31 protects neurons from toxicity induced by MCM. Loss of neuronal MAP-2 stain was measured as a percent of the total area after treatment with MCM at a dilution of 1:5. Loss of MAP-2 immunoreactivity (n=9) mainly reflected loss of processes and was reversed by concurrent treatment with 10 nM LM11A-31 (n=13). *$p<0.05$ t-test, relative to vehicle-treated cells, ** $p<0.05$ t-test, relative to cells treated with MCM only.

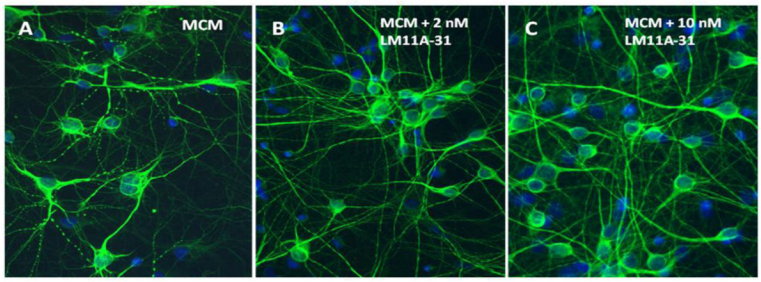

Figure 6.

Neuronal damage produced by 24 h treatment with MCM (1:5) and reversal by LM11A-31. A. Addition of MCM to the neural cultures resulted in dendritic beading and thinning of neuronal processes. B. Co-treatment with 2 nM LM11A-31 partially reversed the beading and loss of processes. C. Co-treatment with 10 nM LM11A-31 reversed the pathology with extensive outgrowth of neuronal processes, indistinguishable from untreated cultures (not shown).

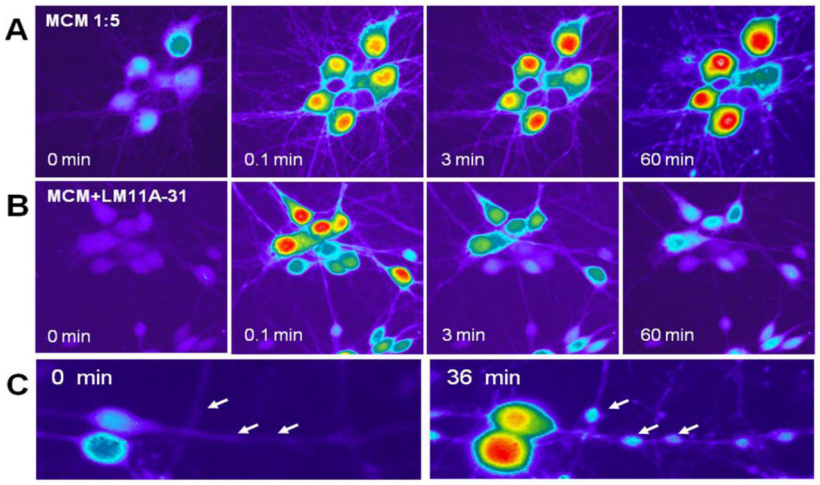

Figure 7.

Example of the calcium response of cultured rat neurons to MCM (1:5) or MCM + LM11A-31 (10 nM). Cells were loaded with Fluo-4 AM and the fluorescence intensity captured and pseudocolored with Metamorph software (white > red > yellow > green > blue > dark blue). Addition of MCM resulted in a large acute calcium response at 0.1 min which failed to recover by 3 min. After 60 min, the neurons were markedly swollen and the processes showed extensive beading. Neurons run in parallel and challenged with the MCM after pre-treatment with LM11A-31 for 10 min showed a comparable acute calcium response followed by substantial recovery by 3 min and no significant delayed calcium rise or pathology. The lower panels illustrate, at high magnification, the development of dendritic beading at 36 min after treatment of neurons with MCM. The beading is accompanied by small local increases in calcium (arrows).

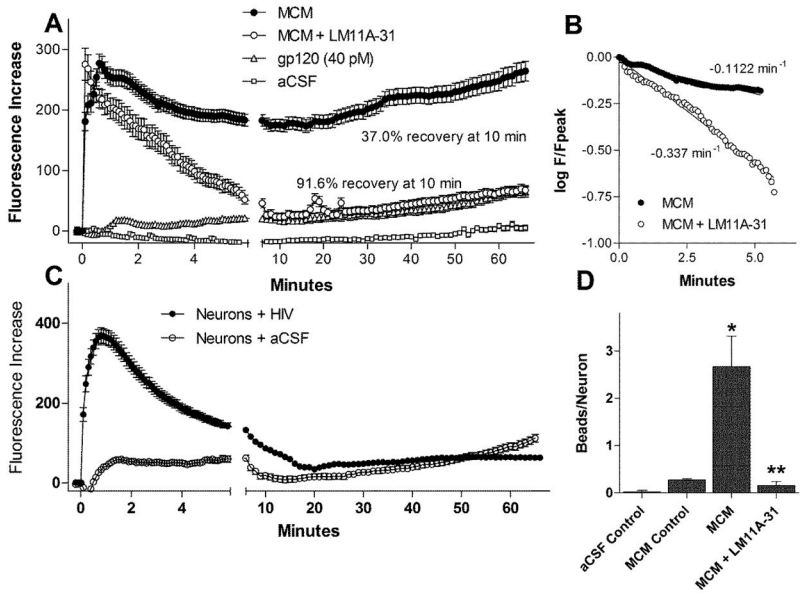

Figure 8.

Reversal of delayed calcium destabilization by LM11A-31. A. Neurons were treated with MCM to generate an acute calcium rise and a delayed calcium destabilization (solid circles). Addition of 10 nM LM11A-31 to the cells 10 min prior to the addition of MCM did not affect the acute calcium response but accelerated calcium recovery and prevented the delayed destabilization. The extent of recovery was limited to 37.0% at 10 min in the MCM challenged cells while the cells pretreated with LM11A-31 showed 91.6% recovery (n=53 neurons). Vehicle (aCSF, n=355) and gp120 (n=28) were run to establish basal calcium dynamics and to control for potential effects of residual gp120. Figures represent results from 4–7 independent experiments. The gp120 evoked a very small acute calcium rise followed by a slight upward drift in intracellular calcium that paralleled the basal calcium response. B. The rate of calcium recovery in neurons treated with MCM with and without LM11A-31 was estimated from the slope of the plot of the log of cell fluorescence at each time point (F) relative to the peak fluorescence (Fpeak). Neurons pretreated with LM11A-31 had a 3-fold increase in the rate of recovery relative to cells treated with MCM alone. C. Conditioned medium from neural cultures treated with HIV gp120 induced an acute calcium response but failed to provoke a delayed destabilization of calcium. D. The number of large swellings (beading) in the processes was negligible in neurons treated with aCSF and slightly increased following incubation in macrophage conditioned medium collected prior to the challenge (MCM control). A large increase in swellings was seen after treatment with MCM which was prevented by concurrent treatment with 10 nM LM11A-31. * p=0.002 t-test vs. MCM control, **p=0.023 t-test, vs. MCM.

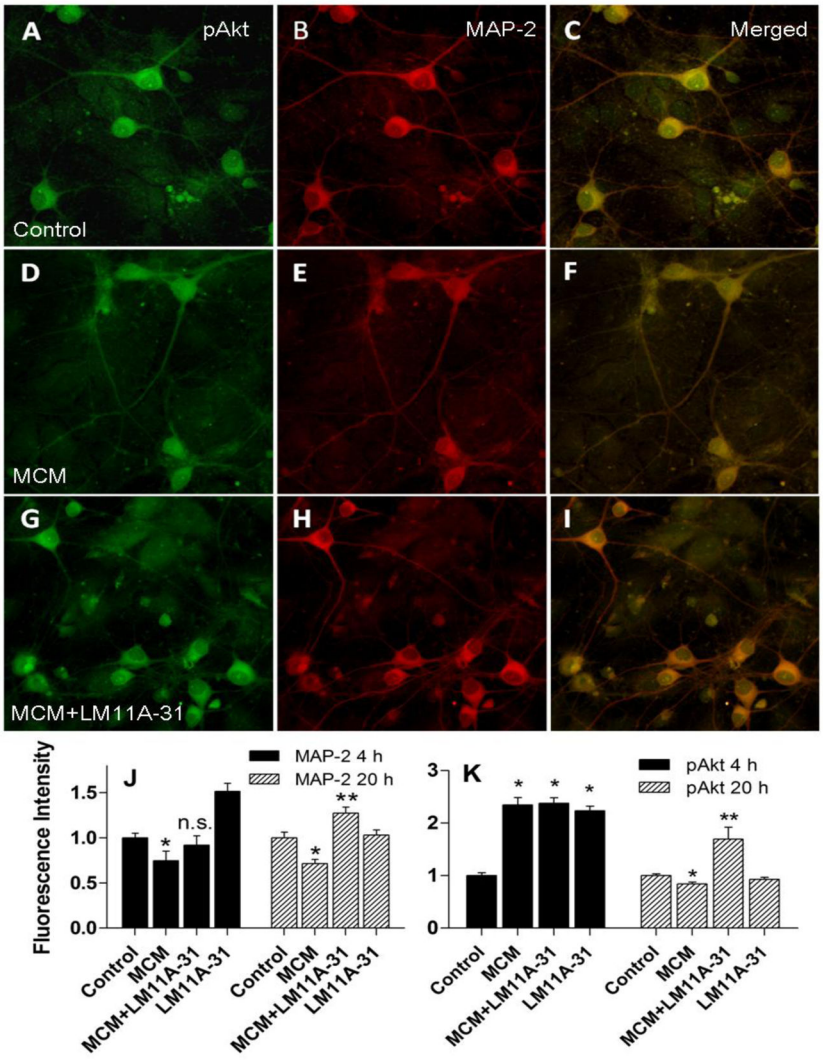

Figure 9.

Neuronal staining for phospho-Akt (pAkt) green and MAP-2 (red) after 20 h treatment with MCM ± LM11A-31. In vehicle treated control neurons, pAkt was seen in the cytosol of MAP-2 stained neurons (A–C) and could also be seen as a weaker stain in astrocytes in the background. Treatment with macrophage conditioned medium (MCM) resulted in a small reduction in the pAkt stain intensity (D–F) which was prevented in the presence of 10 nM LM11A-31 (G–I). J. Quantification of the stain intensity from a total of 47–103 neurons sampled for each condition across 5 different experiments using an unbiased sample template. A two way analysis of variance showed a significant beneficial main effect of MCM + LM11A-31 relative to MCM (all p's < 0.05) which was followed by individual paired comparisons. Four hours after treatment with MCM a 25.1% decrease in MAP-2 immunoreactivity was seen (p=0.020) with a small but non-significant reversal by 10 nM LM11A-31. After 20 h, MAP-2 immunoreactivity was decreased by 28.7%. Co-treatment with 10 nM LM11A-31 completely prevented the loss (p<0.001). At 4 h post-treatment an increase in neuronal pAkt was seen under all conditions (p's<0.001). By 20 h in MCM, a small significant decrease in pAkt expression of 15.6% was seen (p=0.002). In the presence

of MCM+LM11A-31, the expression of pAkt was maintained at a level significantly greater than both control and MCM treated neurons (+69.2 –100.5%, p's<0.001).

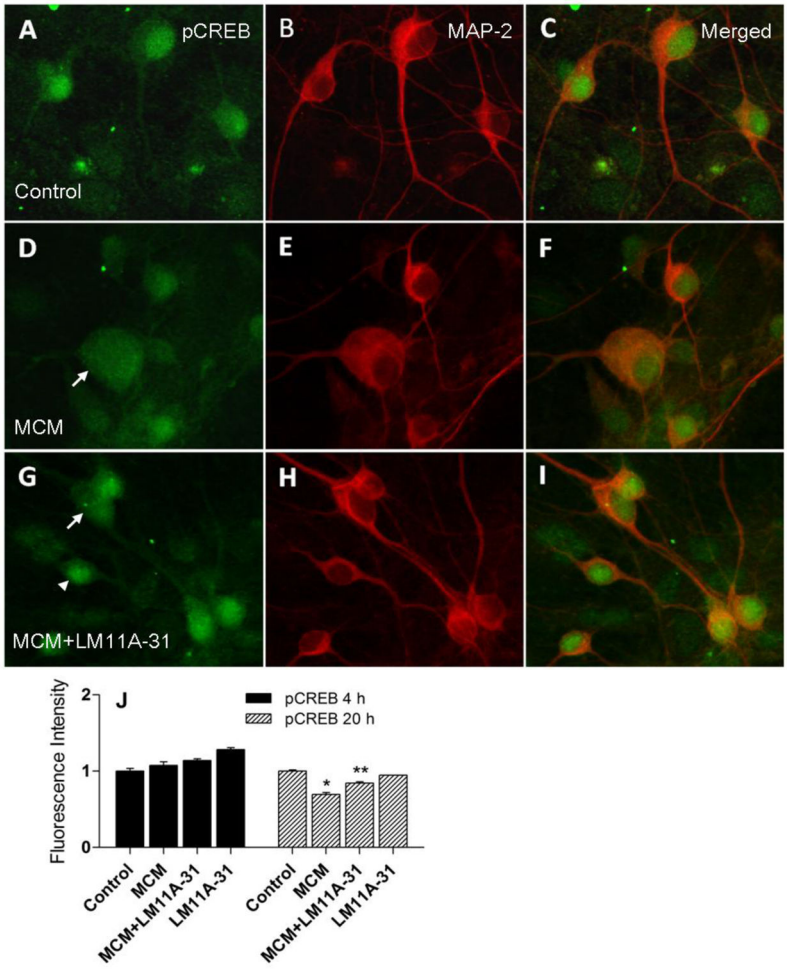

Figure 10.

Neuronal staining for phospho-CREB (pCREB) green and MAP-2 (red) after 20 h treatment with MCM ± LM11A-31. In vehicle treated control neurons, pCREB (A) was preferentially localized to the nucleus of neurons (B, MAP-2) with smaller amounts in the cytosol. C. Merged images showing green nucleus in MAP-2 (red) stained neurons. D–F. Treatment with macrophage conditioned medium (MCM) resulted in a small reduction in the pCREB stain intensity and a loss of nuclear stain in slightly damaged cells (arrow, swollen neuron). The loss of pCREB was prevented in some neurons in the presence of 10 nM LM11A-31 (G, arrowhead) while others showed reduced staining in the nucleus (G, arrow) relative to the cytosol. H–I. MAP-2 intensity was increased by LM11A-31. J. Quantification of the stain intensity from a total of 60–83 neurons sampled for each condition across 5 different experiments using an unbiased sample template. A two way analysis of variance showed a significant beneficial main effect of MCM + LM11A-31 relative to MCM (all p's < 0.05). Individual paired comparisons showed no significant change in neuronal pCREB at 4 h in MCM (+7.4%) or MCM+LM11A-31 (+14.0%). At 20 h post-stimulation, pCREB was decreased relative to untreated controls (−30.6%, $p<0.001$). Addition of 10 nM LM11A-31 to the MCM partially prevented the loss of pCREB (−15.7% $p<0.001$, MCM+LM11A-31 vs. MCM).

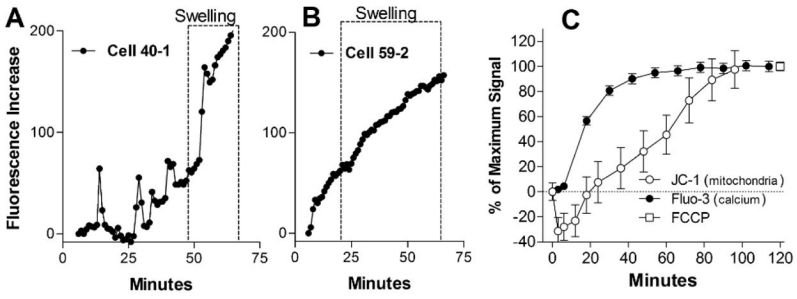

Figure 11.

Time course for the development of mitochondrial depolarization and calcium accumulation in parallel neuronal cultures. Examples of two types of temporal calcium responses in regions of dendritic beading across at least triplicate runs are illustrated in A and B for cell 40-1 and cell 59-2. The box indicates the time during which swelling develops. A. Local regions of dendritic swelling in some neurons exhibited small calcium spikes as early as 14 min post-stimulation followed by a rapid increase (32 min) and swelling (48 min). B. The region of dendritic swelling in other neurons often showed a continuous accumulation of calcium beginning about 20 min prior to the development of swelling. C. Mitochondria were visualized with JC-1 (44 neurons) and neuronal calcium with Fluo-3 (224 neurons). The ratio of green fluorescence to red fluorescence in individual mitochondria within the neuronal cell body was measured to track changes in the mitochondrial membrane potential. Fluo-3 fluorescence intensity was used to track changes in intracellular calcium in matched parallel cultures. To facilitate comparison, fluorescence changes were normalized to the peak change and plotted together. Fluorescence ratios reflecting full mitochondrial depolarization were assessed by adding 1 μM FCCP at the end of the experiment. Destabilization of calcium appeared between 20–40 min, well before changes in the mitochondrial membrane potential. Values represent the mean ± sem.

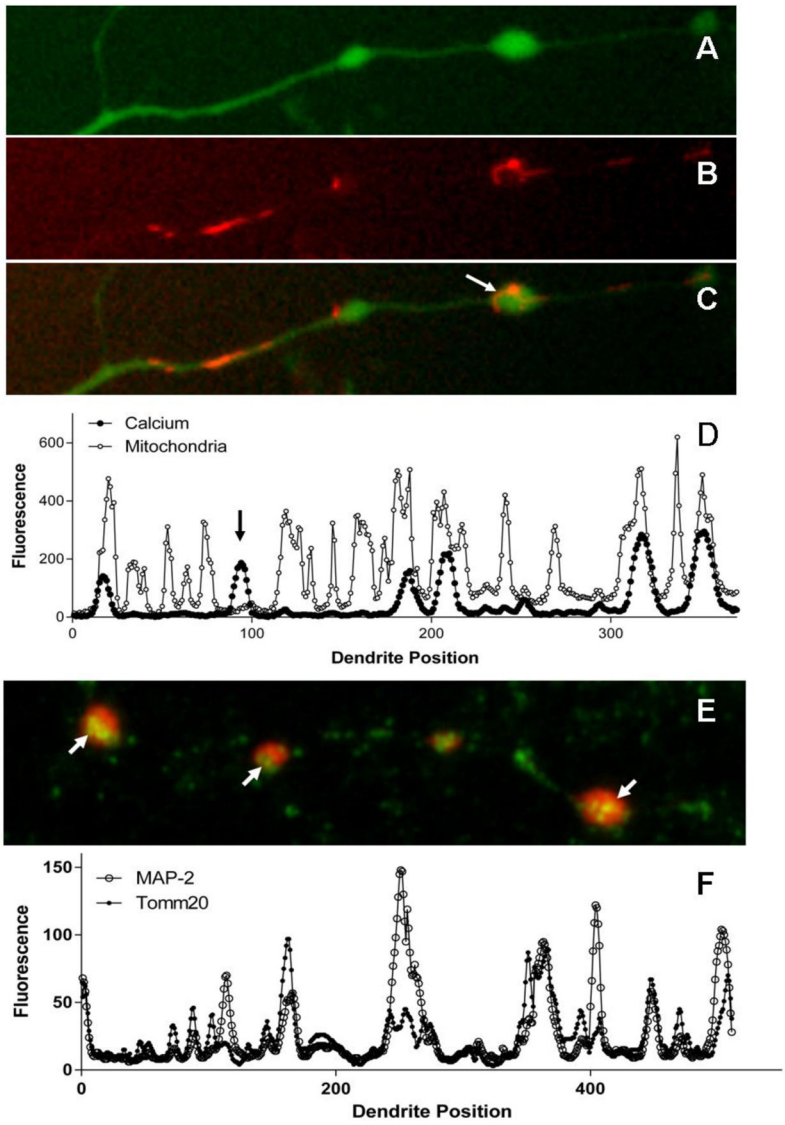

Figure 12.

Comparison of regions of dendrite calcium accumulation and swelling to the location of mitochondria. A. Calcium changes were measured over time in neurons loaded with the indicator Fluo-4 (green). Dendrites with focal swellings were identified in the images, traced and the fluorescence intensity was measured and plotted over the length of the dendrite. B. Mitochondria were stained with 100 nM TMRM (red) for 10 minutes and imaged in the same fashion. C. Merging of the calcium and TMRM stains to show overlap. In some swellings mitochondria appeared to be misoriented (arrow) suggesting a disruption of normal movements. D. The plots of calcium increases (Fluo-4 fluorescence, solid circles) and mitochondrial stain (TMRM, open circles) were superimposed and compared to evaluate the co-localization of the two images. This example shows both overlapping and non-overlapping (arrow) signals from a single representative dendrite. Mitochondria were more abundant that the swellings and were present in many areas with no swelling. Conversely, swellings occasionally had mitochondria present but more typically showed no

TMRM stained mitochondria. E. Tomm20 stain (green) of fixed cells (97% methanol:3% acetic acid) showing mitochondria (green) superimposed on the MAP-2 stained (red) dendrite with prominent swellings (arrows). Overlapping regions appear yellow and often show clusters of mitochondria. Since these cells received the same treatment as A–C above the results indicated that the mitochondria are poorly visible with the membrane potential-dependent stain TMRM. Mitochondria not associated with dendrites (green dots) can be seen in the background. F. The same positional mapping as above showed that almost all swellings (94.3%) contained mitochondria.

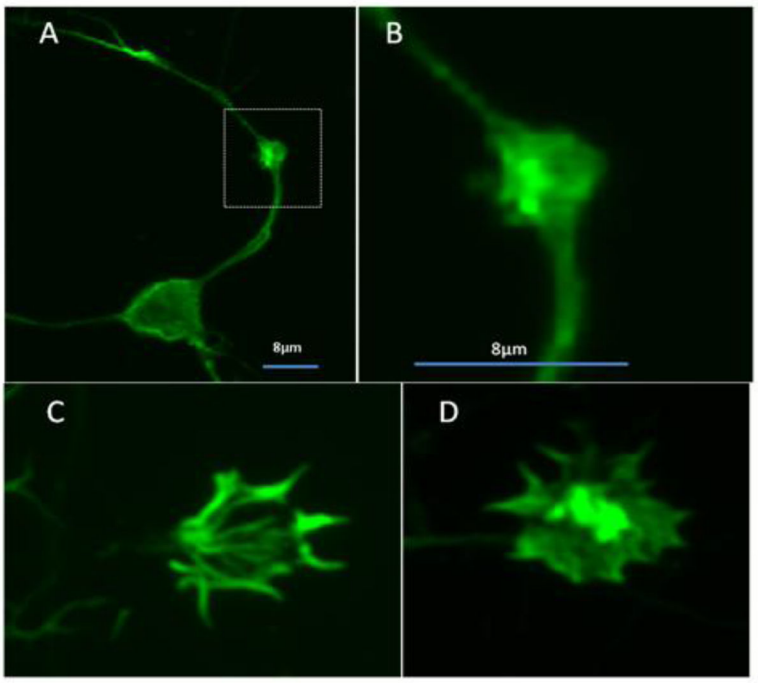

Figure 13.

Accumulation of F-actin aggregates in neurons treated with MCM. A. Example of a dendritic swelling (box) containing a dense accumulation of F-actin stained with phalloidin-Alexa488. B. At high magnification (boxed area in A), the actin appears as amorphous aggregates. Similar aggregates were seen in growth cones from MCM-treated cultures (D) relative to untreated cultures (C).

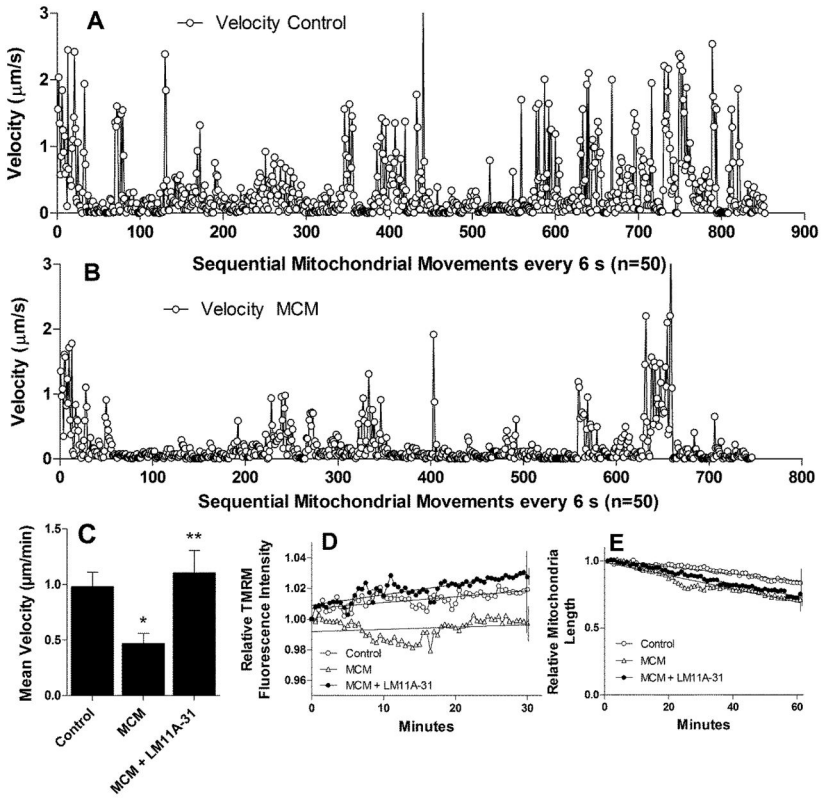

Figure 14.

Mitochondrial movements in neurons are decreased after treatment with MCM and restored by LM11A-31. To measure movements during the period of delayed destabilization of calcium, images were captured 20 min after addition of MCM. A. Successive movements of TMRM stained mitochondria were measured over 6 s intervals in 50 randomly selected mitochondria from normal (aCSF treated) cultures. The velocity of movement was plotted sequentially for each of 1157 epochs where the mitochondria could be clearly tracked. Peaks reflect periods of rapid movement interspersed with periods of slow or no movement. B. After addition of MCM there was a reduction in the number of rapid movements. C. The mean velocity of a total of 200 mitochondria sampled at 20 s intervals from four independent experiments was 0.98 ± 0.13 μm/min in control cultures and was reduced to 0.47 ± 0.09 μm/min in cultures treated with MCM (p=0.002). Addition of 10 nM LM11A-31 with the MCM preserved the movements of the mitochondria (1.10 ± μm/min, p=0.004 vs. MCM). D. The relative intensity of the TMRM, reflecting the mitochondrial membrane potential, did not change significantly over time in the MCM-treated cultured (<2%) and increased slightly (<3%) in MCM+LM11A-31 and control cultures. E. The average relative length of mitochondria decreased slightly in all conditions but no significant differences were seen between conditions.